ELSEVIER

Journal of Fluids and Structures 19 (2004) 511–523

JOURNAL OF FLUIDS AND STRUCTURES

www.elsevier.nl/locate/jnlabr/yjfls

Fluid flow due to a cylinder rolling along ground

S. Bhattacharyya[a], S. Mahapatra[a], F.T. Smith[b,*]

[a] *Department of Mathematics, Indian Institute of Technology, Kharagpur 721302, India*
[b] *Department of Mathematics, University College London, Gower Street, London WC1E 6BT, UK*

Received 25 November 2002; accepted 7 February 2004

Abstract

Planar fluid flow produced by a cylinder rolling over a flat surface is studied, with a view to modelling certain basic effects of a wheel moving uniformly along the ground.This is formulated in terms of a circular cylinder rotating at constant angular velocity, touching and not slipping relative to the moving ground (flat surface). The response near the contact point is obtained analytically and, in conjunction with a transformation, is incorporated in a compact differencing approach. Results are presented over a range of moderate Reynolds numbers, based on the ground speed and cylinder radius, and flow separation properties are discussed.

1. Introduction

The interest here is in the two-dimensional fluid flow induced by a cylinder rolling over a flat surface. The main practical motivation however comes from the automotive industry where there is much concern with the air-flow produced past the wheels of a car or other vehicle. Numerous studies have been made of flows past models, of various degrees of complexity, for cars including the considerable effects from the presence of the ground (Bearman, 1980; Wright, 1982; Katz, 1985a,b; Jacob, 1986; Suh and Ostowari, 1988; Dominy, 1990,1992; Chawla et al., 1990; Jones, 2000; Widnall and Barrows, 1970; Newman, 1982; Tuck and Bentwich, 1983; Plotkin and Dodbele, 1988; Wilson and Duffy, 1998; Jones and Smith, 2003) but it is well known that the wheel effects, which are usually omitted in such studies, are extremely important in practice.

The present work is based on a very simple-minded model of a wheel and its induced flow. Indeed, two-dimensional laminar steady flow of incompressible fluid is assumed. This is bound to miss out many significant features of real wheel flows of course, especially three dimensionality and turbulence, features that are complex individually let alone when acting together. Here a two-dimensional rolling circular cylinder configuration is taken as a starting point. This model puts emphasis on the influence, or part of the influence, due to the lack of relative movement between the ground and the wheel, along with the influence of the contact point between them. The model also has relevance to the rolling of many other obstacles, for example rollers moving under gravity.

Uniform rotation of the circular cylinder on flat ground is assumed. So, in a coordinate frame moving with the constant speed of the centre of the cylinder, the present main task is to determine the flow past a uniformly rotating circular cylinder with a fixed centre and in contact with the ground which travels at a uniform speed, namely the speed of the oncoming free stream of fluid. See Fig. 1.

Many computational as well as analytical and experimental studies have been made of flow past an isolated rotating cylinder in otherwise still fluid, whether for steady or unsteady flow (Glauert, 1957; Moore, 1957; and later works). The additional effects of a free stream have also been addressed (Koromilas and Telionis, 1980; Nikolayev, 1982; Ece et al.,

*Corresponding author. Tel.: +44-20-7679-2837; fax: +44-20-7383-5519.
E-mail address: frank@math.ucl.ac.uk (F.T. Smith).

0889-9746/$ - see front matter
doi:10.1016/j.jfluidstructs.2004.02.003

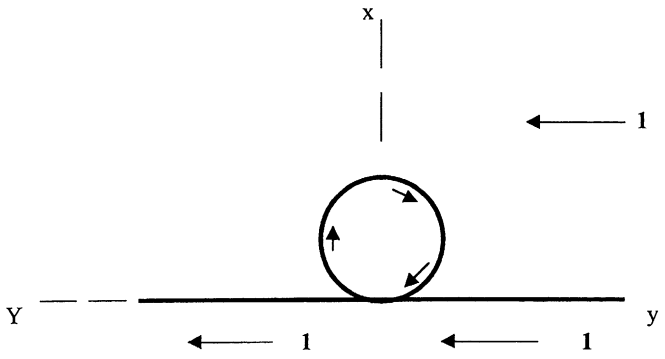

Fig. 1. Schematic diagram of the cylinder rolling along the ground.

1984; Sychev, 1987; Lam, 1988; Chipman and Duck, 1993; Degani et al., 1998). The influence of contact with moving ground, on the other hand, which is central to the present investigation, appears not to have been seriously examined as far as we know. A computational investigation of the model properties is made here in an attempt to provide some insight.

Section 2 describes the formulation of the model problem in nondimensional terms and its response near the contact point in analytical form. The latter is built into the computational approach as presented in Section 3, along with a coordinate transformation and then the application of compact differencing. The results are also presented in that section, over a range of Reynolds numbers based on the ground speed and cylinder radius. Further comments are provided in Section 4.

2. Formulation of model

Two-dimensional laminar steady motion of an incompressible fluid is considered at finite Reynolds number $\mathrm{Re} \equiv U_G r_c/\nu$. Here U_G denotes the dimensional ground speed, r_c is the dimensional radius of the rotating cylinder, whose angular velocity is U_G/r_c, and ν stands for the kinematic viscosity of the fluid. In this formulation the ground moves from right to left and the cylinder rotates clockwise. The nondimensional form to be used is based on U_G, r_c for the velocity components (u, V) and corresponding Cartesian coordinates (x, Y) in turn, and on the product $U_G r_c$ for the associated streamfunction Ψ. This leads to the sketch in Fig. 1 of the configuration in the upper half-plane. We will also use the coordinate y pointing rightward, so that $y = -Y$, with corresponding velocity component $v = -V$ and stream function $\psi = -\Psi$, for convenience.

The continuity and Navier–Stokes equations then take the form

$$u = \frac{\partial \Psi}{\partial Y}, \quad V = -\frac{\partial \Psi}{\partial x}, \tag{2.1a, b}$$

$$u\frac{\partial \zeta}{\partial x} + V\frac{\partial \zeta}{\partial Y} = \frac{1}{\mathrm{Re}}\left(\frac{\partial^2 \zeta}{\partial x^2} + \frac{\partial^2 \zeta}{\partial Y^2}\right), \tag{2.2}$$

where

$$\zeta = -\left(\frac{\partial^2 \Psi}{\partial x^2} + \frac{\partial^2 \Psi}{\partial Y^2}\right) \tag{2.3}$$

is the nondimensional vorticity. The boundary conditions are

$$(\Psi_Y, -\Psi_x) \to (0, 1) \text{ in the farfield}, \tag{2.4}$$

$$-\Psi_x = 1, \quad \Psi = 0 \text{ at } x = 0, \tag{2.5}$$

$$\Psi_r = 1, \quad \Psi = 0 \text{ on } r = 1 \quad (x^2 + Y^2 = 2x). \tag{2.6}$$

Here Eq. (2.4) represents the incident free-stream condition, Eq. (2.5) is the moving-ground condition and Eq. (2.6) is the condition of specified unit rotation speed on the circular cylinder expressed in essence in terms of radial and transverse velocity components measured from the cylinder centre at $(x, Y) = (1, 0)$. Conditions (2.5) and (2.6) confirm

that the cylinder (wheel) does not slip relative to the ground. Here, we assume zero mass flux through/at the contact point.

The problem of Eqs. (2.1)–(2.6) is generally a numerical one, as tackled in the next section for various Reynolds numbers. It is helpful to consider analytically the flow solution near the contact point $(0,0)$. Just to the left of the contact point, where the cylinder surface approximates to $x = x_0(Y) \equiv Y^2/2$, the orders of magnitude involved imply that inertial terms are negligible at leading order and so Eq. (2.2) becomes $\partial^2\zeta/\partial x^2 = 0$ since the $|x|$ scale is substantially smaller than that of $|Y|$. Hence $\zeta = Ax + B$ and Eq. (2.3), which is effectively $\partial^2\Psi/\partial x^2 = -\zeta$, gives $\Psi = -Ax^3/6 - Bx^2/2 + Cx + D$, where A, B, C, D are unknown functions of Y. The four requirements in Eqs. (2.5) and (2.6), with the latter applying on $x = x_0$, then determine A, B, C, D to be $12/x_0^2, -6/x_0, -1, 0$ respectively. In consequence the asymptotic form

$$\Psi \sim -8x^3 Y^{-4} + 6x^2 Y^{-2} - x \tag{2.7}$$

applies locally. As a check, for small $|x|$, Eq. (2.7) yields Ψ of order $|x|$ and hence V is of order unity from Eq. (2.1), in keeping with the prescribed ground and rotation speed. Further ζ is therefore of order $|x|^{-1}$ and so, in Eq. (2.2), $V\partial\zeta/\partial Y$ and $\partial^2\zeta/\partial x^2$ have the respective orders $|x|^{-3/2}$ and $|x|^{-2}$.Thus the viscous terms are indeed dominant as

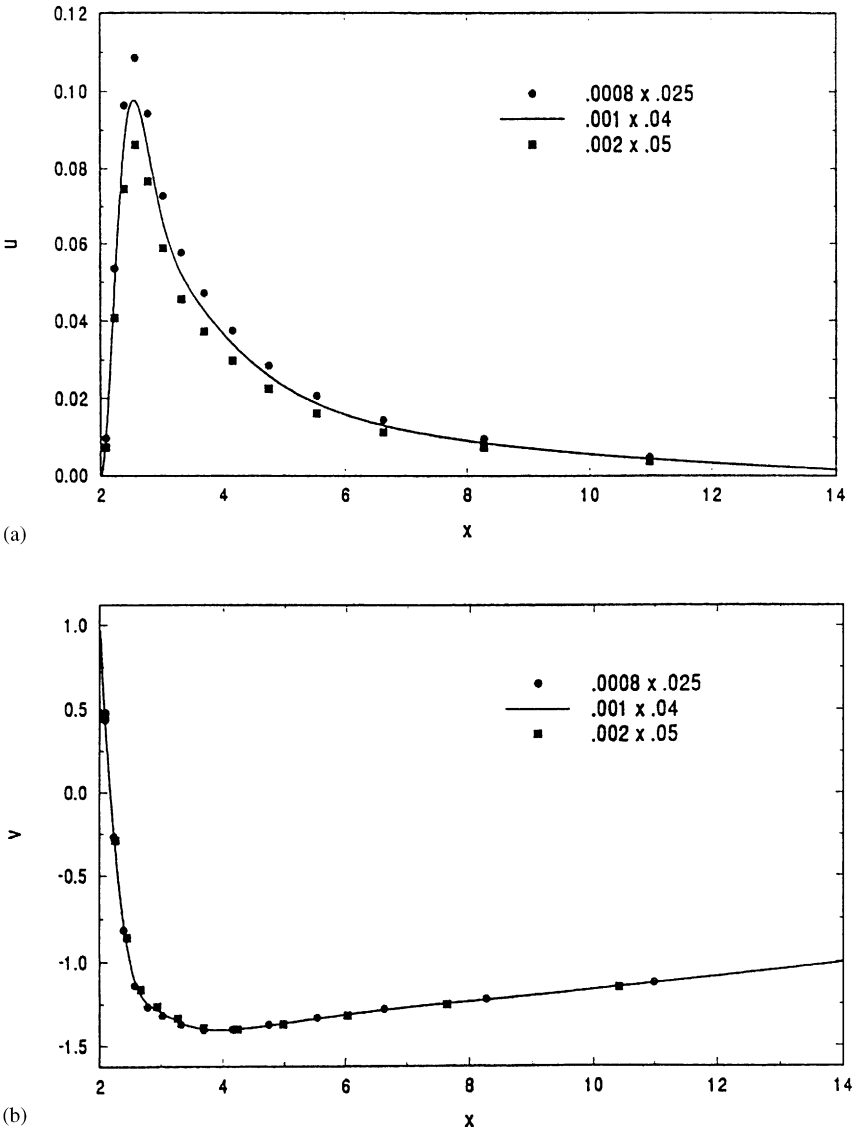

Fig. 2. Effect of step size on velocity profiles along $y = 0$ line: (a) u-velocity profile; (b) v-velocity profile.

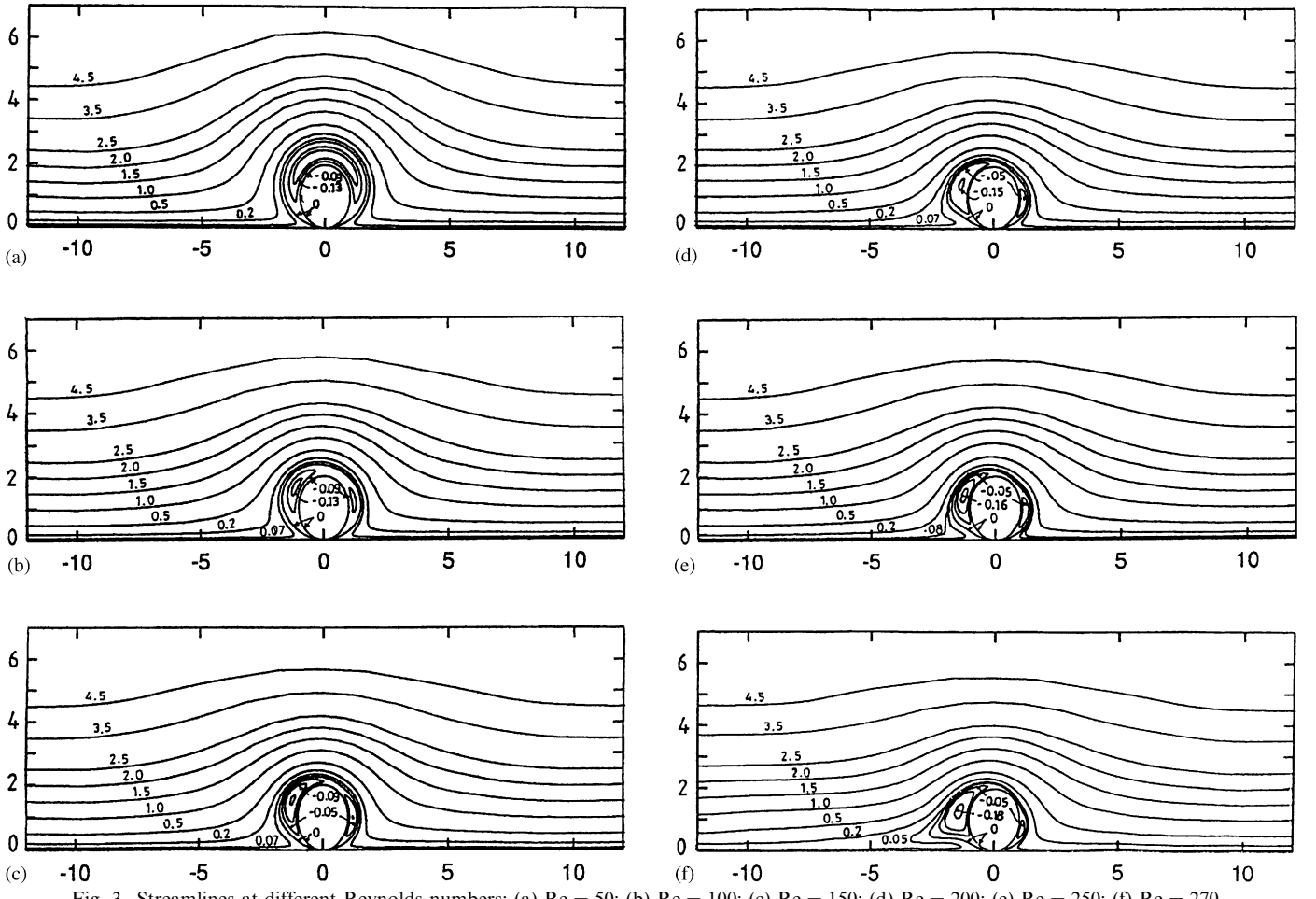

Fig. 3. Streamlines at different Reynolds numbers: (a) Re = 50; (b) Re = 100; (c) Re = 150; (d) Re = 200; (e) Re = 250; (f) Re = 270.

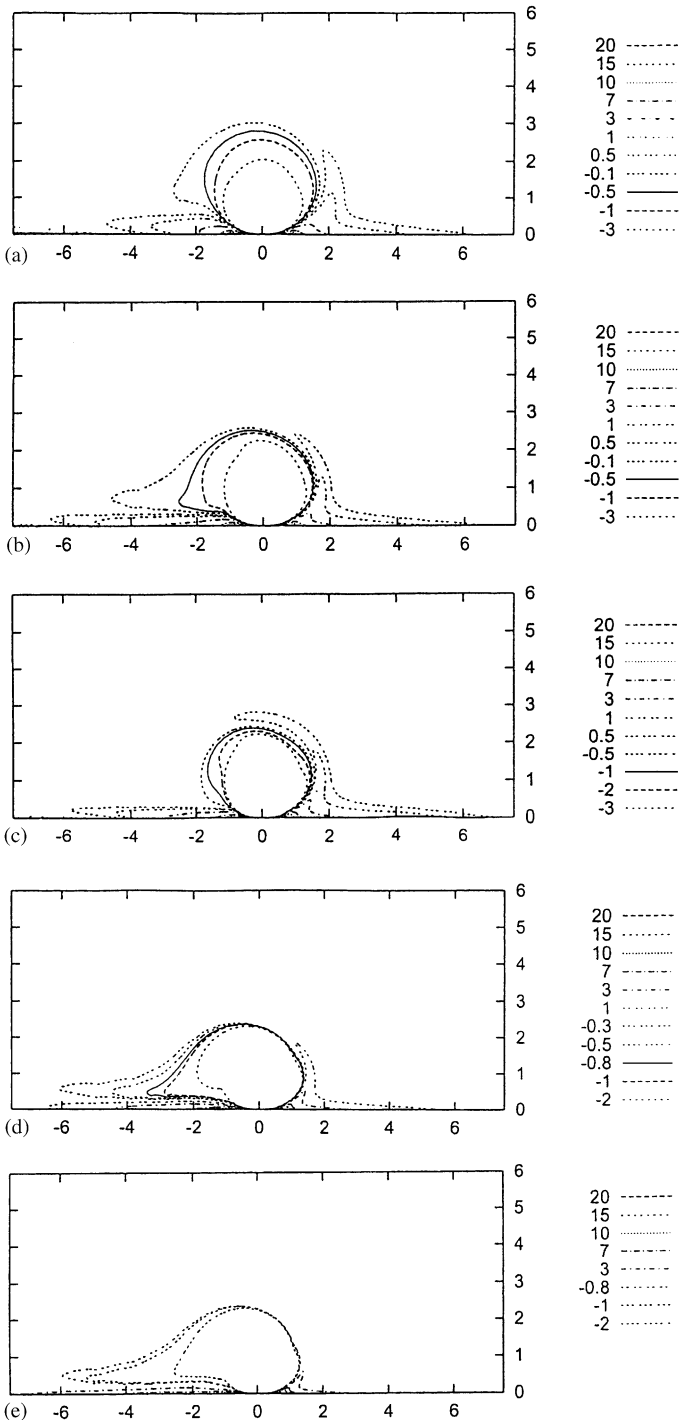

Fig. 4. Vorticity contours at different Reynolds numbers: (a) Re = 50; (b) Re = 100; (c) Re = 150; (d) Re = 200; (e) Re = 250.

assumed above, albeit only by a factor $|x|^{1/2}$. Just to the right of the contact point, similarly, Eq. (2.7) again holds. The local behaviour in Eq. (2.7) is used below. It is of interest that the corresponding local form for the velocity profile is

$$V \sim 24x^2 Y^{-4} - 12x Y^{-2} + 1, \tag{2.8}$$

which yields a reversing jet-like profile as expected from continuity, i.e., some fluid is forced to flow away from the contact point, just to the right of contact, whereas some is drawn towards the contact point on the left side. The zeros of v according to Eq. (2.8) occur at the two positions $x/Y^2 = (1 \pm 1/\sqrt{3})/4$ between the ground ($x = 0$) and the cylinder ($x/Y^2 = \frac{1}{2}$).

3. Computational method and results

On the numerical side, a transformation was first made to enable the use of more convenient coordinates, namely the complex form

$$w = z^{-1}. \tag{3.1}$$

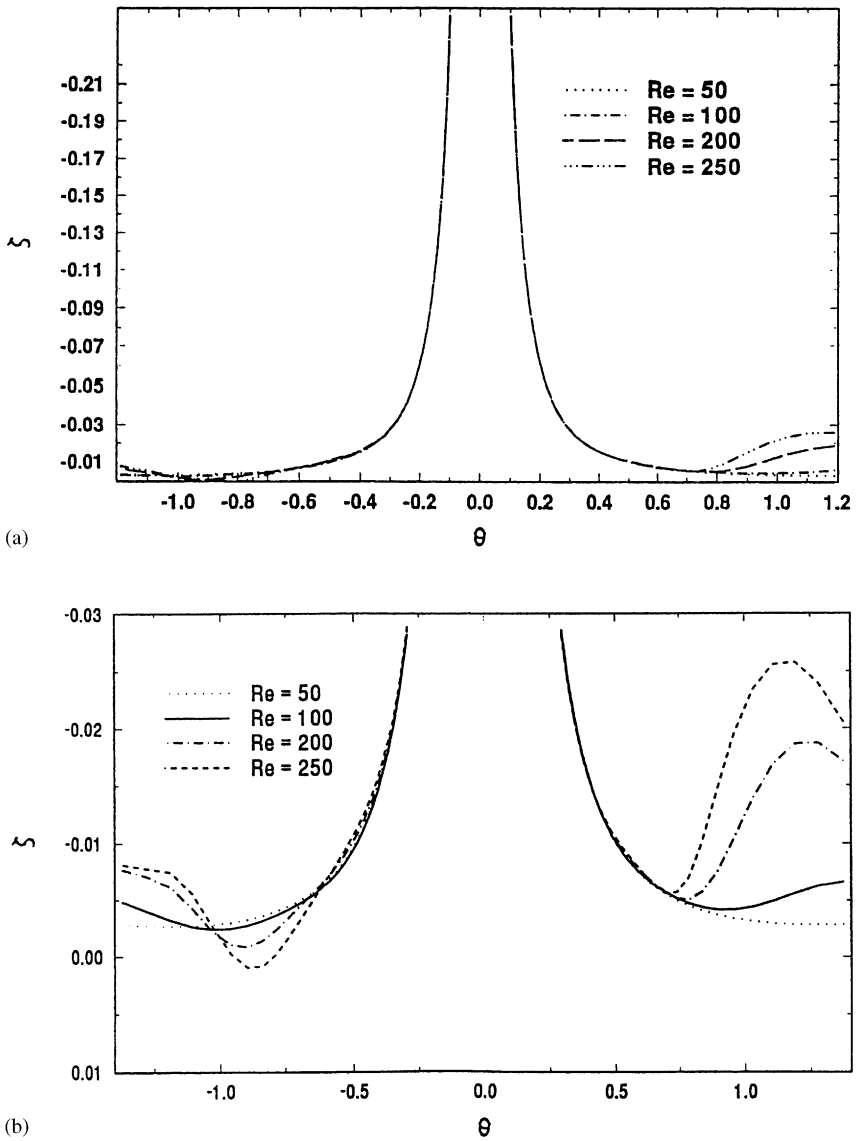

Fig. 5. (a) Vorticity along the wheel surface at different Reynolds numbers. (b) A magnified view of the surface vorticity away from the point of contact.

Here $w = \xi + i\eta$ is the new working plane and $z = x + iY$ is the physical plane. With Eq. (3.1) holding, the problem of Eqs. (2.1)–(2.6) becomes that of solving

$$\left(\frac{\partial \Psi}{\partial \eta}\frac{\partial}{\partial \xi} - \frac{\partial \Psi}{\partial \xi}\frac{\partial}{\partial \eta}\right)\zeta = \frac{1}{\mathrm{Re}}\left(\frac{\partial^2 \zeta}{\partial \xi^2} + \frac{\partial^2 \zeta}{\partial \eta^2}\right), \tag{3.2}$$

$$\zeta = -(\xi^2 + \eta^2)^2\left(\frac{\partial^2 \Psi}{\partial \xi^2} + \frac{\partial^2 \Psi}{\partial \eta^2}\right) \tag{3.3}$$

for ζ, Ψ as functions of ξ, η in the strip $0 \leqslant \xi \leqslant \frac{1}{2}$, $-\infty < \eta < \infty$, with the conditions

$$\Psi = 0 \text{ on } \xi = 0, \quad \xi = \frac{1}{2}, \tag{3.4}$$

$$\Psi_\xi = -\eta^{-2} \text{ on } \xi = 0 \quad \text{for all } \eta, \tag{3.5}$$

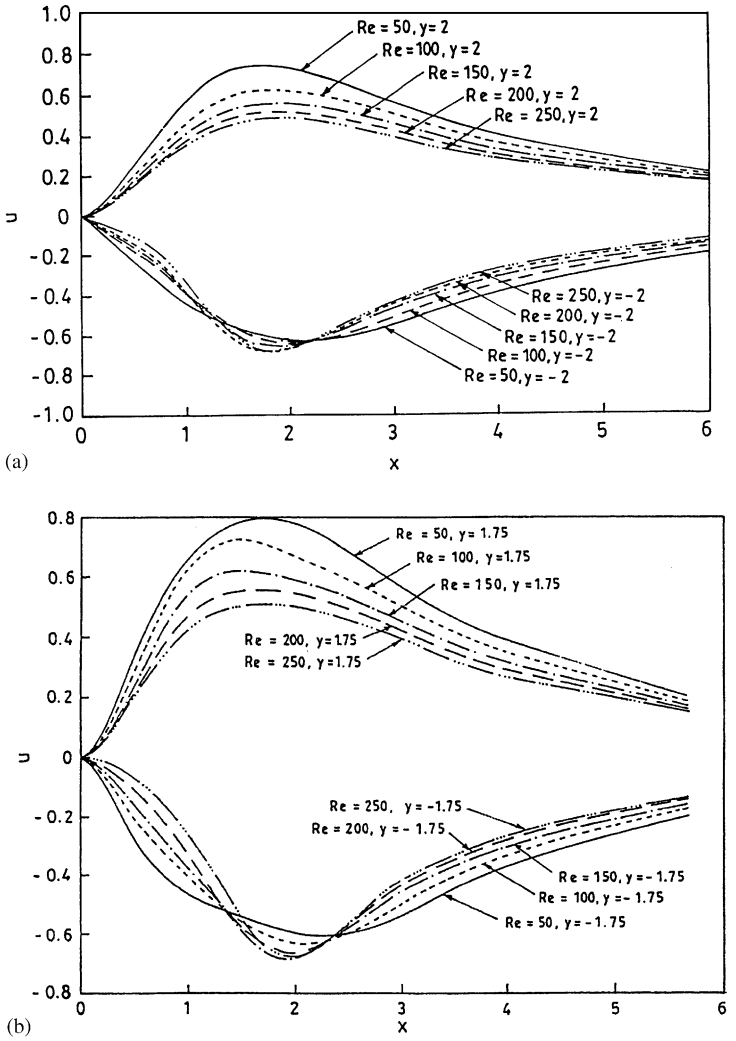

Fig. 6. Velocity profiles at different x, y stations for different values of Reynolds number, $\mathrm{Re} = 50, 100, 150, 200, 250$: (a) u-velocity at $y = 2.0, -2.0$; (b) u-velocity at $y = 1.75, -1.75$; (c) v-velocity at $y = 1.75, -1.75$; (d) u-velocity at $y = 1.25, -1.25$; (e) v-velocity at $y = 1.25, -1.25$; (f) u-velocity at $y = 1, -1$; (g) v-velocity at $y = 1, -1$; (h) u-velocity at $y = 0$ for the range $x \geqslant 2$; (i) v-velocity at $y = 0$ for $x \geqslant 2$.

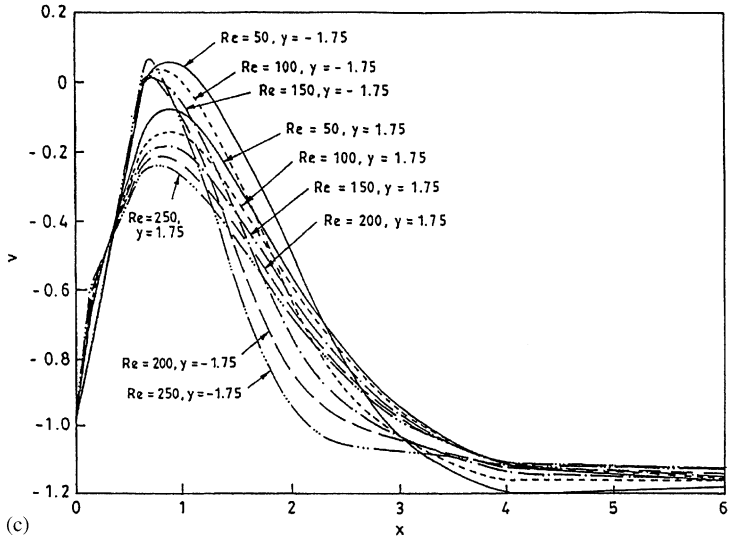

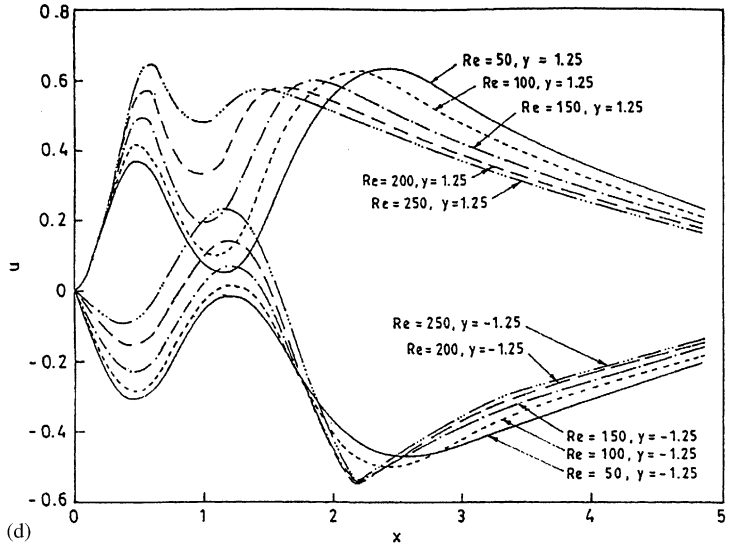

Fig. 6 (*continued*).

$$\Psi_{\xi} = -\left(\eta^2 + \frac{1}{4}\right)^{-1} \quad \text{on } \xi = \frac{1}{2} \quad \text{for all } \eta, \tag{3.6}$$

$$\Psi \sim -\xi/(\xi^2 + \eta^2) \text{ as } (\xi, \eta) \to (0, 0). \tag{3.7}$$

Conditions (3.4)–(3.6) are from the ground and cylinder constraints in Eqs. (2.5) and (2.6), while condition (3.7) stems from the incident stream Eq. (2.4), in the physical far field which is of course the origin in the w-plane. Also, the asymptotic behaviour

$$\Psi \sim -\frac{\xi}{\eta^2}(8\xi^2 - 6\xi + 1) \text{ as } |\eta| \to \infty, \quad \text{for } 0 \leqslant \xi \leqslant \tfrac{1}{2} \tag{3.8}$$

is inferred from Eq. (2.7) near the point of contact.

A compact-difference method was then applied. In this steady problem a fictitious time derivative is introduced in the vorticity Eq. (3.2) and each time step is considered equivalent to an iteration. The time derivative is discretized through

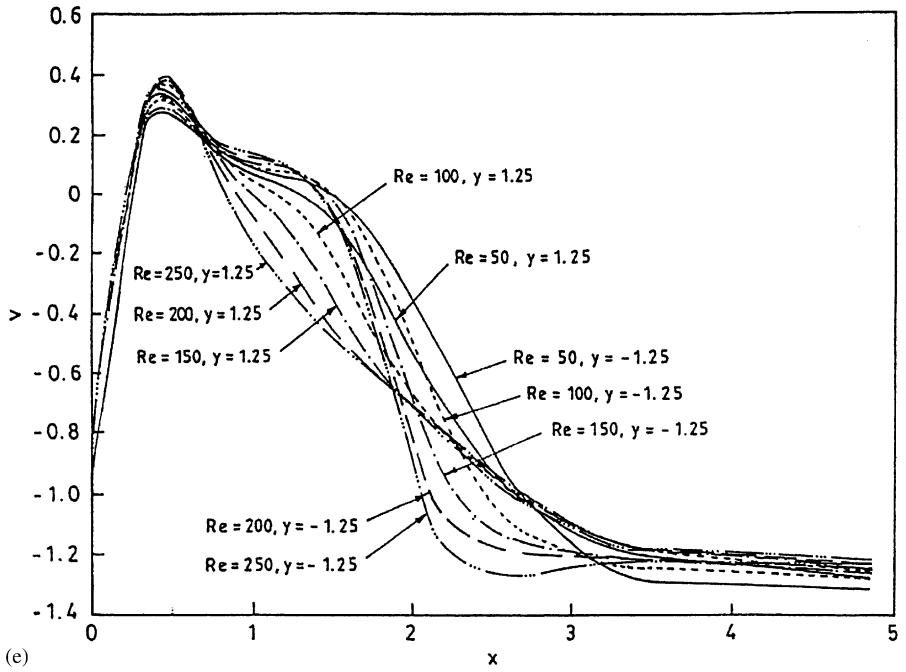

(e)

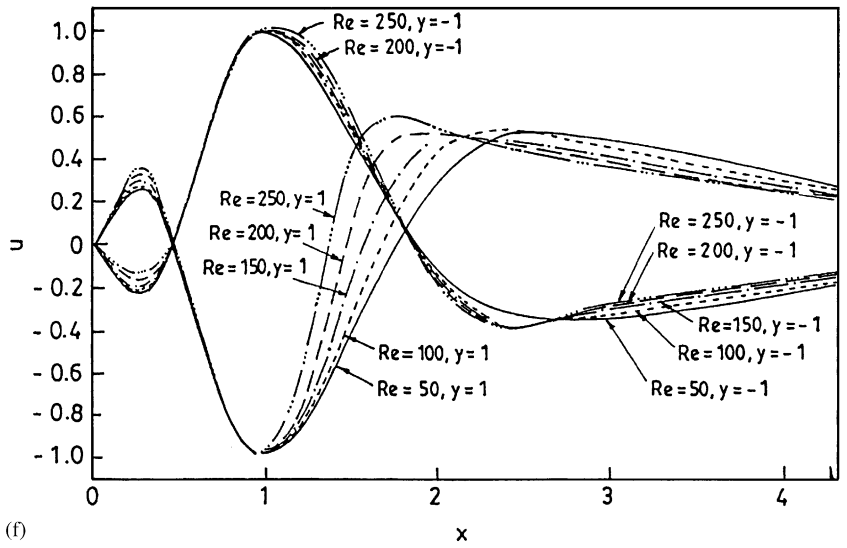

(f)

Fig. 6 (*continued*).

an alternating-direction-implicit scheme (ADI). In order to satisfy the numerical stability criteria for flow with strong flow reversal, a third-order upwind difference scheme is used in the convective terms. At every fractional time step the stream function is updated by solving Eq. (3.3) through a fourth-order accurate compact difference scheme. This fourth-order method considers as unknowns at each discretized points not only the value of the function but also its first and second derivatives. The system is closed by considering a set of fourth order accurate relations. We used this scheme earlier to study the flow past a surface mounted obstacle [Bhattacharyya et al. (2001), where a detailed discussion of the numerical scheme is given]. In the present computational domain the origin is enclosed by a semi-circle.

In order to check the grid dependence of our results, we varied the grid sizes $\delta\xi$ and $\delta\eta$ in the ξ and η directions between 0.0008×0.025 and 0.002×0.05, respectively. Because of the complex transformation in Eq. (3.1), the grid

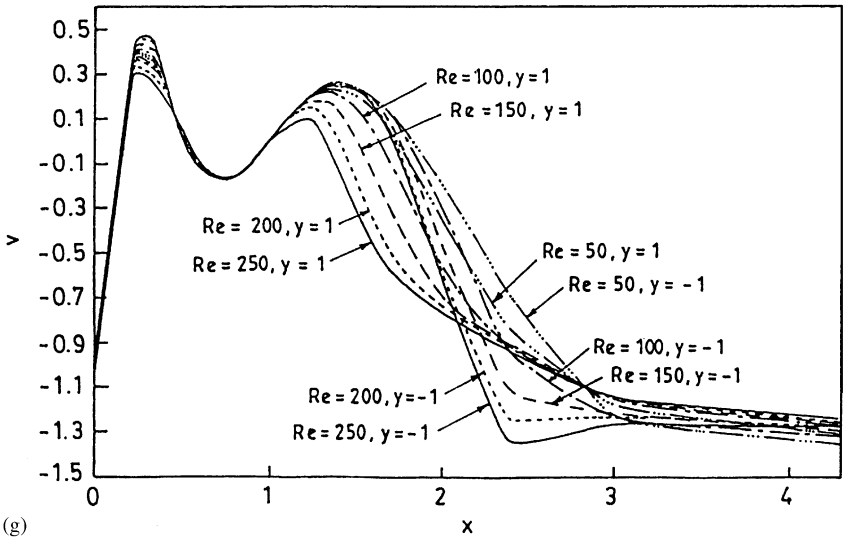

(g)

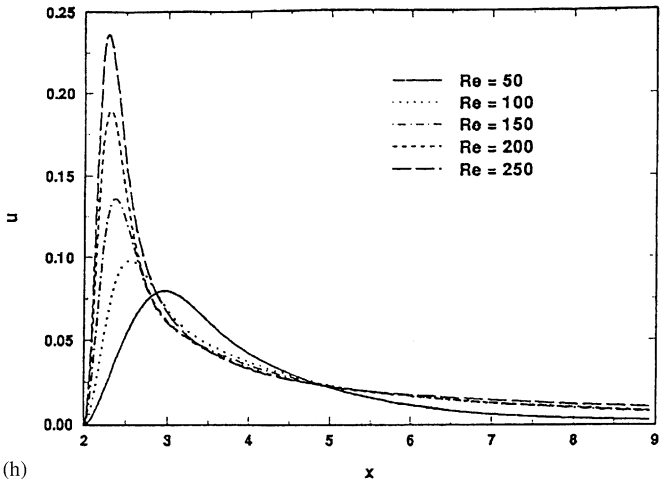

(h)

Fig. 6 (*continued*).

points become dense near the point of contact. We choose $\delta\xi$ much smaller than $\delta\eta$. Fig. 2(a) and (b) shows the effects of grid size on the velocity profile along the $y = -Y = 0$ line in the physical plane. We found that a uniform grid of size $\delta\xi = 0.001$ in the ξ direction and $\delta\eta = 0.04$ in the η-direction is near optimal.

We present the streamlines, vorticity contours and velocity profiles at different values of Reynolds number, typically values $\mathrm{Re} = 50, 100, 150, 200, 250$, in the xy-plane. The computational results clearly show that a massive change in flow pattern occurs in the region around the wheel (cylinder). Streamline patterns at different values of Reynolds number are presented in Fig. 3(a)–(f). The streamlines are reversed near the surface of the wheel. The stagnation streamline ($\psi = -\Psi = 0$) is almost circular for $\mathrm{Re} < 200$. For higher values of Reynolds number ($\mathrm{Re} > 200$), the region of oppositely rotating fluid (anticlockwise) on the downstream side of the wheel is higher than on the upstream side. Adjacent to the wheel there are some closed regions of recirculating fluid. The recirculating fluid velocity increases with an increase of Reynolds number over the present range. It is clear from the figures that the rotation of the wheel also affects the flow field far above the wheel centre. The iso-vorticity contours at different values of Reynolds number Re, from 50 to 250, are presented in Fig. 4(a)–(e). We find that the vorticity along the sliding ground is positive, whereas the vorticity in the apparent boundary layer around the rotating wheel is negative. The thickness of the boundary layer on the upstream side of the wheel reduces with an increase of Re. However, increasing Re increases the thickness of the

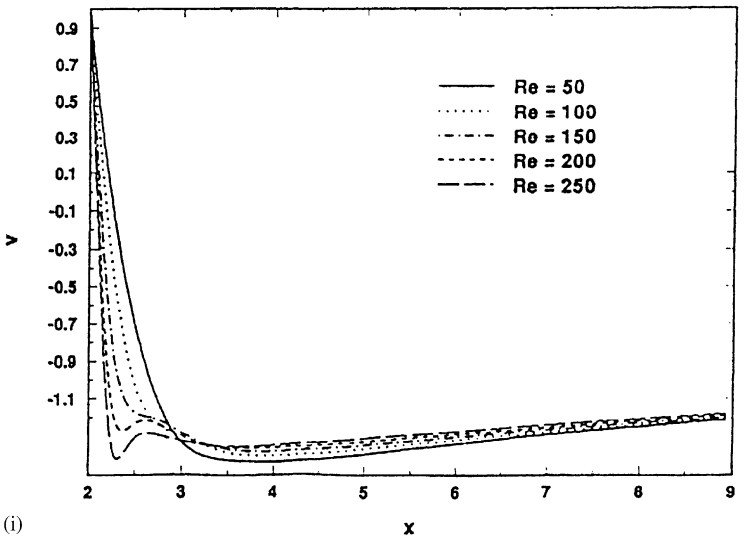

(i)

Fig. 6 (*continued*).

boundary layer on the downstream side of the wheel. A shear layer is formed on the upstream side of the wheel. The thickness of this shear layer decreases as the Reynolds number increases.

The vorticity along the surface of the wheel is presented in Fig. 5(a) for $\mathrm{Re} = 50, 100, 200, 250$. The surface vorticity values are scaled by the highest value of the surface vorticity. The surface vorticity is highest at the point of contact of the wheel with the ground. Along the upstream side of the wheel $\theta = \tan^{-1}(x/y)$ varies from zero (at the point of contact) to $\pi/2$ (highest point) and along the downstream side θ varies between zero to $-\pi/2$. A magnified view of the region away from the point of contact where the vorticity changes rapidly is displayed in Fig. 5(b). This shows clearly that the surface vorticity results on the upstream and downstream sides are far from symmetric for $\mathrm{Re} \geqslant 100$.

Velocity profiles are presented in Fig. 6(a)–(i) at different x, y locations for $\mathrm{Re} = 50$ to 250. Far upstream of the wheel Fig. 6(a) and (b) at $y = 2, 1.75$ show that the vertical velocity u is positive (upwards flow) and on the downstream side at $y = -2, -1.75$ the vertical velocity is all negative (downwards flow). At $y = \pm 1.75$ the horizontal velocity v is all negative (Fig. 6(c)). There the magnitude of v rapidly decreases and becomes very close to zero within a small distance above the ground. Fig. 6(d) and (e) show the velocity profiles at $y = \pm 1.25$.These indicate that at such y values the horizontal velocity v becomes positive in a narrow region above the ground. This positive v increases with an increase of Re. Fig. 6(d) shows that the vertical velocity u is oscillatory. At $y = 1.25$ (upstream side) the vertical velocity is upwards. The vertical velocity is predominantly downwards at $y = -1.25$ (downstream side). Both the velocity profiles have a monotonic nature away from the surface of the wheel where $x > 2$. The magnitude of the upward or downward vertical velocity decreases with distance away from the wheel.

Close to the surface of the wheel ($y = \pm 1$), the horizontal velocity v on the upstream side is away from the wheel ($v > 0$) and is towards the wheel on the downstream side for $0.2 < x < 1.25$, i.e., in a region just above the point of contact of the wheel with the ground. The horizontal velocity v is negative except in the region $0.2 < x < 1.25$.The velocity profiles exhibit oscillations near the wheel surface. On the upstream side ($y = 1$), Fig. 6(f) shows the vertical velocity u is positive (upwards) in the region close to the point of contact ($0 < x < 0.5$) whereas u is negative (downwards) on the downstream side ($y = -1$). The plots of v at $y = 1$ and -1 indicate (see Fig. 6(g)) that the horizontal velocity v becomes positive in a region just above the point of contact. This quite clearly indicates that near the point of contact of the wheel with the ground, part of the fluid is thrown away from the wheel on the upstream side whereas an inward jet exists on the downstream side. The computational result is in agreement with the flow analysis described in Section 2. Fig. 6(f) shows that in the region near $x = y = 1$, above the point of contact on the upstream side of the wheel, a strong downward flow exists whereas the flow is upward on the downstream side near $x = 1$, $y = -1$. The velocity profiles immediately above the wheel, i.e. along the $y = 0$ line for $x \geqslant 2$, are presented in Fig. 6(h) and (i). They show that close to the wheel surface both u and v are positive, i.e. the fluid is thrown away from the wheel. The horizontal velocity v decreases steadily in general apart from some undershooting and becomes negative above the wheel surface.

4. Further comments and conclusion

The results of the previous section cover a range of moderate Reynolds numbers but the flow solutions appear to be rich in structure. They indicate clearly that a massive change in flow pattern occurs in the region around the surface of the wheel (cylinder). In particular they show significant flow separation as might be expected, occurring on the downstream side of the rotating cylinder despite the presence of an inflow jet produced toward the point of contact on that side (Sections 2 and 3) and an outflow jet on the upstream side. As far as properties for increasing Reynolds numbers are concerned, the findings tend to point to ideas based on interactive boundary layers coupled with large-scale inviscid separated flow models. It would nevertheless be of some interest to examine the classical attached form with assumed potential flow almost everywhere. The steady case then would seem to have limited relevance but the unsteady case may exhibit lift-off of the viscous effects similar to that in the Degani et al. (1998) study. Again, although high shear stresses are induced near the contact point, as shown in Section 2 and the results of Section 3, the local behaviour there is actually of lubrication type and so is free of inertia. This is in contrast with a potential flow model.

Further study on the free rolling of a cylinder under gravity down an inclined plane for instance is called for. Likewise the influence of nonzero mass flux is of concern at the contact point, due to leakage acting on a smaller lengthscale. However, to repeat, the model investigated in the present work is a simple one and in particular its extension to three-dimensional motion represents a significant challenge.

Acknowledgements

Support from EPSRC (UK) for S.B. on a visiting fellowship to University College London is gratefully acknowledged.

References

Bearman, P.W., 1980. Bluff body flows applicable to vehicle aerodynamics. In: Morel, T., Dalton, C. (Eds.), Aerodynamics of Transportation, ASME, New York.

Bhattacharyya, S., Dennis, S.C.R., Smith, F.T., 2001. Separating shear flow past a surface-mounted obstacle. Journal of Engineering Mathematics 39, 47–62.

Chawla, M.D., Edwards, L.C., Franke, M.E., 1990. Wind-tunnel investigation of wing-in-ground effects. Journal of Aircraft 27, 289–293.

Chipman, P.D., Duck, P.W., 1993. On the high Reynolds number flow between non-coaxial rotating cylinders. Quarterly Journal of Applied Mathematics 46, 163–192.

Degani, A.T., Walker, J.D.A., Smith, F.T., 1998. Unsteady separation past moving surfaces. Journal of Fluid Mechanics 375, 1–38.

Dominy, R.G., 1990. The influence of slipstreaming on the performance of a Grand Prix racing car. Journal of Automobile Engineers (Proceedings of the Institution of Mechanical Engineers) 204, 35–40.

Dominy, R.G., 1992. Aerodynamics of a Grand Prix racing car. Journal of Automobile Engineers (Proceedings of the Institution of Mechanical Engineers) 206, 267–274.

Ece, M.C., Walker, J.D.A., Doligalski, T.D., 1984. The boundary layer on an impulsively started rotating and translating cylinder. Physics of Fluids 27, 1077–1089.

Glauert, W.B., 1957. The flow past a rapidly rotating circular cylinder. Proceedings of the Royal Society London A 242, 108–115.

Jacob, K., 1986. Advanced method for computing flow around wings with rear separation and ground effect. Journal of Aircraft 24, 126–128.

Jones, M.A., 2000. Mechanisms in wing-in-ground effect aerodynamics. Ph.D. Thesis, University of London.

Jones, M.A., Smith, F.T., 2003. Fluid motion for car undertrays in ground effect. Journal of Engineering Mathematics 45, 227–245.

Katz, J., 1985a. Investigation of negative lifting surfaces attached to an open-wheel racing car configuration. International Congress & Exposition Detroit, Michigan, USA; SAE Technical Paper 850283.

Katz, J., 1985b. Calculation of the aerodynamic forces on automobile lifting surfaces. ASME Journal of Fluids Engineering 107, 438–443.

Koromilas, C.A., Telionis, D.P., 1980. Unsteady laminar separation:an experimental study. Journal of Fluid Mechanics 97, 347–384.

Lam, S.T., 1988. On high-Reynolds-number laminar flows through a curved pipe, and past a rotating cylinder. Ph.D. Thesis, University of London, UK.

Moore, D.W., 1957. The flow past a rapidly rotating cylinder in a uniform stream. Journal of Fluid Mechanics 2, 541–550.

Newman, N., 1982. Analysis of small-aspect-ratio lifting surfaces in ground effect. Journal of Fluid Mechanics 117, 305–314.

Nikolayev, K.V., 1982. Boundary-layer separation on a rotating cylinder in the flow of an incompressible fluid. Uchenye Zpiski, The Central Aerohydrodynamics Institute 3, 32–39.

Plotkin, A., Dodbele, S.S., 1988. Slender wing in ground effect. AIAA Technical Note 26, 493–494.
Suh, Y.B., Ostowari, C., 1988. Drag reduction factor due to ground effect. Journal of Aircraft 25, 1071–1072.
Sychev, V.V., 1987. Ivd. Akad. Sci. SSSR Mekhanika Zhidk. Gaza 43.
Tuck, E.O., Bentwich, M., 1983. Sliding sheets: lubrication with comparable viscous and inertia forces. Journal of Fluid Mechanics 135, 51–69.
Widnall, S.E., Barrows, T.M., 1970. An analytical solution for two- and three-dimensional wings in ground effect. Journal of Fluid Mechanics 41, 769–792.
Wilson, S.K., Duffy, B.R., 1998. On lubrication with comparable viscous and inertia forces. Quarterly Journal of Mechanics and Applied Mathematics 51, 105–124.
Wright, P.G., 1982. The influence of aerodynamics on the design of Formula One racing cars. International Journal of Vehicle Design 3, 383–396.